UCLA

UCLA Previously Published Works

Title

Upper Limb Redundancy Resolution Under Gravitational Loading Conditions: Arm Postural Stability Index Based on Dynamic Manipulability Analysis

Permalink

https://escholarship.org/uc/item/2p71214x

Authors

Shen, Yang
Hsiao, Brandon Po-Yun
Ma, Ji
et al.

Publication Date

2017-11-15

Data Availability

The data associated with this publication are available upon request.

Peer reviewed

Upper Limb Redundancy Resolution Under Gravitational Loading Conditions: Arm Postural Stability Index Based on Dynamic Manipulability Analysis

Yang Shen, Brandon Po-Yun Hsiao, Ji Ma, and Jacob Rosen

Abstract— Resistance training may be considered as one promising approach for improving the motor capabilities of post-stroke patients. A successful introduction of this depends on the proper resolution of human arm redundancy under gravitational loading. The spatially heterogeneous changes of the human arm swivel angle (which represents the upper limb redundancy) are studied under different loading conditions, the effects of which are incorporated into a modified dynamic manipulability ellipsoid model. A new scalar index describing the arm postural stability (APSI) is then proposed. As part of the experimental protocol, ten (10) healthy subjects performed multiple reaching tasks with different weights mounted on the forearm. Kinematic data was collected via a ten-camera motion capture system and the corresponding APSI was calculated for each task. APSI is found to have a strong linear correlation with the swivel angle under loading conditions. Furthermore, the data suggest that the swivel angle may serve as an indicator of arm postural stability and task difficulty. The results of additional experiments conducted with three (3) subjects indicate that the external loads could deteriorate the arm's control performance in tasks like line tracing (root mean square deviation from straight lines). These findings may be applicable to robot-based (exoskeleton) resistance therapy, assist-as-needed gravity compensation, and human-like motion control of humanoid robotic systems.

Index Terms— Redundancy resolution, human upper limb, rehabilitation robotics, manipulability, resistance training.

I. INTRODUCTION

A. Background

Stroke is one leading cause of severe long-term disability [1]. Among different post-stroke rehabilitation strategies, resistance training like coupled bilateral load exercises have shown positive evidence in improving motor capabilities of the impaired upper limb and additional investigations are needed [2], [3]. On the other hand, rehabilitation robots like the exoskeleton system shown in Fig. 1 have been developed to automate the training process by providing controllable and repetitive motion [4], [5]. Surprisingly, although resistance controllers have been reported in manipulanda-like training devices, no robotic exoskeleton has this feature available [6]. To the authors' knowledge, this is because:

- Unlike manipulanda devices which are manipulated using hands, multi-link exoskeletons usually have multiple contact points with the human arm. The redundancy

The authors are with Department of Mechanical and Aerospace Engineering, University of California Los Angeles, 420 Westwood Plaza, Los Angeles, CA 90095, USA yang_shen@engineering.ucla.edu, {branpyhsiao, jima, jacobrosen}@ucla.edu
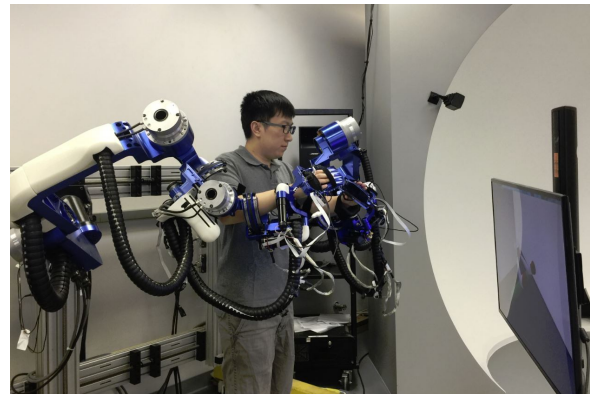
Fig. 1. A subject operates the EXO-UL8, a dual-arm exoskeleton system developed in the authors' lab, with seven degrees of freedom (7 DOFs) and one hand gripper on each side, to perform tasks in virtual reality.

and temporal/spatial synergies existing in human arm movement bring more uncertainty and complexity.
- Many rehabilitation exoskeletons are originally developed to provide assistance rather than resistance (e.g., pre-defined trajectories). To achieve good human-robot interaction transparency, joint torque output capabilities are often compromised by system backdrivabilities.

Given that both the human arm and exoskeleton have a redundant degree-of-freedom (DOF), one question that needs to be answered for achieving high human-robot transparency in resistance training is whether external resistance changes the natural redundancy resolution strategy of the human arm and thus provides referential information to the exoskeleton controller. Although applications of virtual reality could visualize different force directions, this study, as a starting point, considers external loadings as the only resistance since additional weights deteriorate performance in activities of daily living (ADLs): intuitively, swiping cards, rotating a doorknob, and waving hand become more difficult when a heavy bag is hanging on the arm.

To quantitatively characterize the effect of additional loading, a modified dynamic manipulability ellipsoid is used. Traditionally studied in robotics research, the manipulability models have been applied back to human motion analysis and proven effective. Table I provides examples of past research ranging from rehabilitation robotics to ergonomics. However, no study on upper limb considered the effect of gravity when using a manipulability model.

TABLE I

EXAMPLES OF RESEARCH USING MANIPULABILITY MODELS

Anatomical Interests	Example Studies	Manipulability Models	Resistance/Loads	Applications
Upper Limb	Sasaki *et al.*, 2010 [7]	MFE, FP	N	Wheelchair Operations
	Jacquier-Bret *et al.*, 2012 [8]	DME, FP	N	Upper Limb Movement Capabilities
	Tanaka *et al.*, 2015 [9]	HFM	N	Operational Comfort
Lower Limb	Walsh *et al.*, 2006 [10]	N/A	Y(Loads)	Load-Carrying Augmented Exo
	Gordon *et al.*, 2009 [11]	N/A	Y(Loads)	Hip Kinetics & EMG
	Yu *et al.*, 2012 [12]	MM, ME	N	Assistive Mechanism Design
Hand/Fingers	Gupta *et al.*, 2008 [13]	MM	N	Wrist Rehabilitation
	Valero-Cuevas, 2009 [14]	MFE, FP	N	Neuromuscular Control
	Endo, 2015 [15]	MM, ME	N	Smartphone Touch Operations

B. Main Contributions

- For the first time, this paper quantitatively discusses the spatial heterogeneity of human arm redundancy resolution (swivel angle) due to gravitational resistance;
- A new scalar arm postural stability index (APSI), is proposed. Its high correlation with swivel angles is observed when additional loads are present. We conjecture that the swivel angle under loading conditions may work as an indicator of arm postural stability/task difficulty.

The rest of the paper is arranged as: Part II gives detailed mathematical modeling of a 2-link 4-DOF human arm; Part III describes the experiments including two tasks; Part IV provides results and discussion; Part V concludes the paper.

II. MODELING

A. Modified Dynamic Manipulability Ellipsoid

First proposed by Yoshikawa [16], the manipulability measure (MM) and its visualization - the manipulability ellipsoid (ME) have been modified and extended to versions like the "dynamic manipulability ellipsoid (DME)" [17], the "manipulability force ellipsoid (MFE)" [18] and the "manipulability velocity ellipsoid (MVE)" [19]. Considering the effect of loading as well as the relatively low arm moving speed during post-stroke upper limb rehabilitation training, the authors adopted and extended a modified DME model [20], the derivation of which is provided as follows.

First, a serial (with actuators at each joint) manipulator's dynamics could be described as:

$$M(\mathbf{q})_{n \times n} \ddot{\mathbf{q}}_{n \times 1} + \mathbf{c}(\mathbf{q}, \dot{\mathbf{q}})_{n \times 1} + \mathbf{g}(\mathbf{q})_{n \times 1} + J^T(\mathbf{q})_{n \times m} \mathbf{f}_{m \times 1} = \boldsymbol{\tau}_{n \times 1} \tag{1}$$

where the torque vectors $M(\mathbf{q})_{n \times n} \ddot{\mathbf{q}}_{n \times 1}$, $\mathbf{c}(\mathbf{q}, \dot{\mathbf{q}})_{n \times 1}$ and $\mathbf{g}(\mathbf{q})_{n \times 1}$ are inertia, Coriolis/centrifugal, and gravity-related terms, respectively. $J^T(\mathbf{q})_{n \times m}$ is the transpose of Jacobian matrix linking end-effector force vector $\mathbf{f}_{m \times 1}$ and joint torque vector $\boldsymbol{\tau}_{n \times 1}$. $J(\mathbf{q})_{m \times n}$ also links joint space (n-DOF) velocity with task space (m-DOF) velocity:

$$\dot{\mathbf{x}}_{m \times 1} = J(\mathbf{q})_{m \times n} \dot{\mathbf{q}}_{n \times 1} \tag{2}$$

A non-redundant, unconstrained stationary assumption ($m = n, \dot{\mathbf{q}} = \mathbf{0}, \mathbf{f} = \mathbf{0}$) simplifies (1) to (3), and the time derivative of (2) to (4).

$$M \ddot{\mathbf{q}} + \mathbf{g} = \boldsymbol{\tau} \tag{3}$$

$$\ddot{\mathbf{x}} = J \ddot{\mathbf{q}} = J M^{-1} \boldsymbol{\tau} + \ddot{\mathbf{x}}_g \tag{4}$$

where:

$$\ddot{\mathbf{x}}_g = -J M^{-1} \mathbf{g} \tag{5}$$

represents the translation of ellipsoid center away from original end-effector position. To the authors' best knowledge, this translation has never been quantitatively analyzed or applied in previous related research, although it could help determine if the arm wrist is already out of the dynamic manipulability ellipsoid and if making gravity compensation necessary. Details are discussed later in this section. Historically, for simplicity researchers assume that the manipulator's torque capability could be normalized using $\tilde{\boldsymbol{\tau}} = T^{-1} \boldsymbol{\tau}$, $T = diag(\tau_{1,max}, ..., \tau_{n,max})$ as the scaling matrix and represented by a unit sphere (Euclidean norm) in joint space (6) and then a distorted/rotated ellipsoid could be calculated and visualized in task space (7), indicating the feasible acceleration directions and magnitudes.

$$\tilde{\boldsymbol{\tau}}^T \tilde{\boldsymbol{\tau}} \leq 1 \tag{6}$$

$$(\ddot{\mathbf{x}} + J M^{-1} \mathbf{g})^T J^{-T} Q J^{-1} (\ddot{\mathbf{x}} + J M^{-1} \mathbf{g}) \leq 1 \tag{7}$$

where:

$$Q = M T^{-2} M \tag{8}$$

In this study, the 2-link 2-DOF non-redundant robotic manipulator model example in [17] is extended to a 2-link 4-DOF redundant human arm model, and an index indicating the arm postural stability is later proposed in II. B.

Illustrated in Fig. 2, following the Y-X-Z rotation order at the center of the (right) shoulder, the elbow and wrist joint positions $P = [\mathbf{P_e}, \mathbf{P_w}]$ are calculated in the base frame (9), with q_1 to q_4 representing shoulder extension(+)/flexion(-), shoulder adduction(+)/abduction(-), shoulder internal(+)/external(-) rotation, and elbow extension(+)/flexion(-), respectively. L_1 and L_2 represent the lengths of upper arm and forearm respectively. For simplicity, $c \cdot := cos(q \cdot)$ and $s \cdot := sin(q \cdot)$:

$$P = \begin{bmatrix} -s1c2L_1 & -(s1s2s3 + c1c3)s4L_2 - s1c2(L_1 + c4L_2) \\ s2L_1 & -c2s3s4L_2 + s2(L_1 + L_2c4) \\ -c1c2L_1 & -(c1s2s3 - s1c3)s4L_2 - c1c2(L_1 + c4L_2) \end{bmatrix} \tag{9}$$
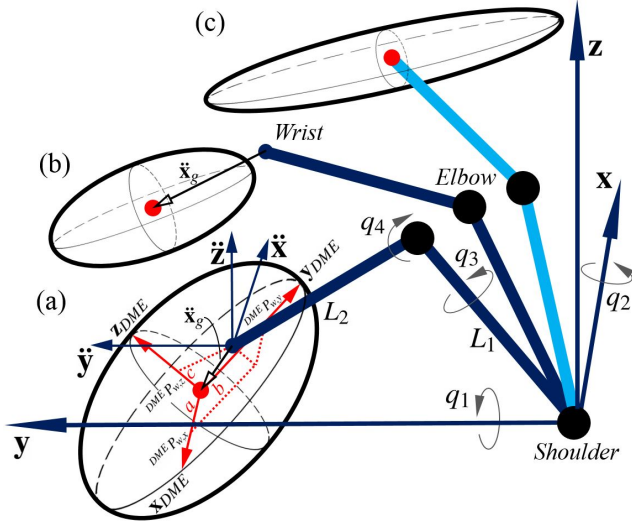
Fig. 2. The DMEs of a 2-link 4-DOF arm: (a) with loading, $0 < s < 1$; (b) with loading, $s < 0$; (c) no loading, $s = 1$. A local coordinate system for DME is built on $\mathbf{x}_{DME}$, $\mathbf{y}_{DME}$ and $\mathbf{z}_{DME}$, along major, intermediate, and minor axes respectively. The DME's size/orientation/position change with arm configurations and loading.

Due to the redundancy, the dynamic manipulability ellipsoid (10) uses a weighted pseudoinverse of Jacobian $J_Q^\dagger = Q^{-1}J^T(JQ^{-1}J^T)^{-1}$ (with $J_{3\times4}$ detailed in Appendix):

$$(\ddot{\mathbf{x}} + JM^{-1}\mathbf{g})^T J_Q^{\dagger T} Q J_Q^\dagger (\ddot{\mathbf{x}} + JM^{-1}\mathbf{g}) \leq 1 \qquad (10)$$

This represents the modified dynamic manipulability ellipsoid for a redundant 2-link 4-DOF human arm in its 3-DOF task space. Any vector starting from the wrist and ending within the ellipsoid visualizes an acceleration (with magnitude and orientation) that the arm could achieve. As the ellipsoid center moves under loading conditions (5), once large enough loads are applied to the arm the ellipsoid no longer encompasses the wrist. In this case, the wrist loses the ability to move in at least half of the directions, and the arm configuration is theoretically no longer stable. To quantify the change from stable (no loads, ellipsoid centers at wrist) to unstable (large loads, ellipsoid no longer encompasses the wrist), we propose a scalar index below.

B. Arm Postural Stability Index (APSI)

A singular value decomposition (SVD) on the core of (10), $N = J_Q^{\dagger T} Q J_Q^\dagger$ provides three eigenvalues ($\sigma_{1,2,3}$, which determine the ellipsoid size and volume used as traditional manipulability measure) and the corresponding eigenvectors which determine the ellipsoid orientation. Using the translation equation (5), any arm configuration is labeled with a scalar index $\in (-\infty, 1]$ shown below (11). The index is proposed to quantify arm postural stability (i.e., APSI) when loads are present:

$$APSI = 1 - \sqrt{(^{DME}P_{w,x}/a)^2 + (^{DME}P_{w,y}/b)^2 + (^{DME}P_{w,z}/c)^2} \qquad (11)$$

where $a = 1/\sqrt{\sigma_1}$, $b = 1/\sqrt{\sigma_2}$ and $c = 1/\sqrt{\sigma_3}$ are the semi-axis lengths of the DME. The wrist position in the DME

coordinate frame, $^{DME}\mathbf{P_w}$ is calculated by (12):

$$^{DME}\mathbf{P_w} = R^{-1}(-\ddot{\mathbf{x}}_g) = -R^{-1}JM^{-1}\mathbf{g} \qquad (12)$$

where $R_{3\times3}$ is a rotational matrix based on the eigenvectors of N. Geometrically, the APSI represents the normalized distance to ellipsoid boundary. If $APSI \leq 0$ (Fig. 2(b)), the configuration is theoretically unachievable or unstable as the wrist position is out of the ellipsoid and only a small portion of feasible acceleration directions is left. If $0 < APSI \leq 1$ (Fig. 2(a)), the wrist is within the ellipsoid and thus the configuration is achievable. As the APSI gets closer to 1, the arm is supposed to have higher postural stability, e.g., APSI = 1 in Fig. 2(c), when loading is not considered. Notice that the units of the DME coordinate system are different from those of the Cartesian one. For visualization purposes, the DME coordinate system is scaled. Therefore, one could tell if the DME encompasses the wrist only by the method given in (11), rather than by visual comparison.

C. Parameter Estimation

To reduce interference in natural arm movement, loads will be applied on the forearm only, with the center of mass (CoM) located L_{c2} from the elbow. The upper arm and forearm masses are m_1 and m_2 respectively. Estimated from [7], [21]: $L_{c2} = 0.3m$, $m_1 = 2.44kg$, $m_2 = 1.40kg$, $T = diag(35, 50, 30, 20)Nm$. Based on [22], the anatomical joint angles (in deg) are limited by: $q1 \in [-120, 0]$, $q2 \in [-100, 20]$, $q3 \in [-40, 60]$, and $q4 \in [-130, -10]$.

III. EXPERIMENT

A. Subjects

Ten (three females and seven males) healthy, right-handed adults participated (mean $\pm$ s.d.; age: 22.50 $\pm$ 2.59y, weight: 66.70 $\pm$ 8.31kg, height: 174.60 $\pm$ 8.30cm). All ten accomplished Task I; three of ten (#1-male, #2-female, #7-female) were randomly selected to accomplish the additional Task II.

B. Setup

Fig. 3(a) provides an overview of the experiment setup. Based on the subjects' average range of motion (ROM) in the task space, the targets are evenly positioned in a reachable 3×3 matrix, parallel to the subject's frontal plane, at two different distances (*close* and *far*), marked on the ground (same to all subjects). The subject, wearing reflective markers on hand, elbow and shoulder, is asked to sit against the backrest of an armless chair to constrain the movement of his/her trunk. 3-D kinematics of the right upper limb is recorded at 100Hz by ten cameras of a motion capture system (Vicon, UK).

C. Task I (Reach-Out Arm Posture)

Redundancy resolution remains an open question, especially when with loads. Illustrated in Fig. 3(b), if one keeps the shoulder and wrist positions unchanged, s/he could still change the elbow position to some extent, along a circle perpendicular to a line connecting the shoulder and wrist. This redundant DOF, represented by an angle swiped by
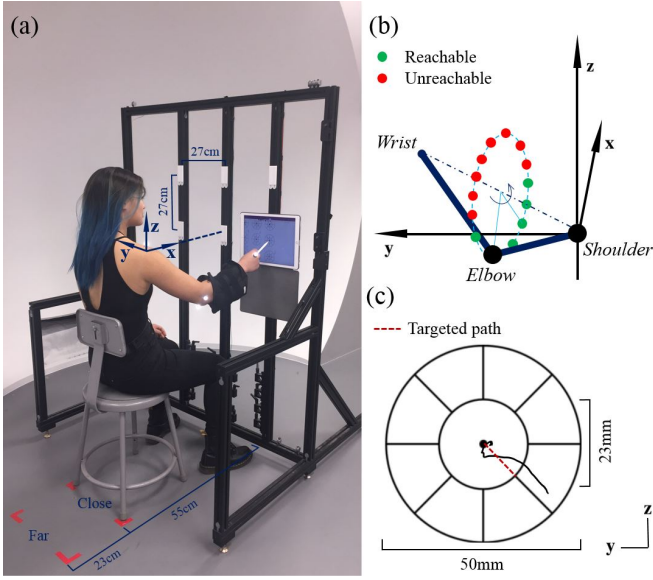
Fig. 3.   (a) Experiment setup: one subject is using a stylus to accomplish Task I & II, the targets (white) are positioned so that the x-axis on right shoulder points to the center of 3×3 target matrix; (b) Swivel angle (Task I): looking from shoulder to wrist, positive swivel angle starts from lowest elbow position counterclockwise (i.e., elbow rotates away from the body); (c) Target (center) and sub-tasks (Task II): the subject has finished the subtask from center to (0,-1,-1) direction. The targeted path is later added for image processing and not shown to subjects. The deviation is calculated from center to inner circle only.

the elbow and starting counterclockwise from the zero point where the elbow is lowest in Cartesian space, is called "swivel angle". Each subject is loaded with three different weights: 0, 2.72, and 4.54kg (= 0, 6, and 10lb). This is done by wrapping weight adjustable sandbags (CAP Barbell, USA) on the subject's forearm. The subject is asked to rest his/her right arm on his/her lap and once s/he receives a "start" instruction, reach and touch the target with a stylus (gripped between forefinger and middle finger) using elbow and shoulder movements only, hold for 3 seconds and rest the arm back. After a 10-second-break, the subject moves to the next target and repeats the above until all nine targets are touched. A different load is then applied. Once all three loads are tested, the subject moves to the other distance. The swivel angles at the targets are individually calculated, based on the marker positions. After each session, a 10-min-break is provided.

D. Task II (Arm's Control Performance in Drawing Task)

Similarly, with two different loads: 0 and 2.72kg (= 0 and 6lb), the subjects are asked to reach and touch the target using the same stylus as described in Task I. The difference is, once the target is reached, the subject is asked to draw a line segment from the target center to any sub-target marked along the inner circle of the target (Fig. 3(c), 23mm in diameter), every 45 degrees. Then the stylus goes back to the center without drawing anything, and repeats the drawing task to another sub-target until all eight sub-targets are connected to the center. The subtasks are done in the subject's preferred order. The images drawn on the
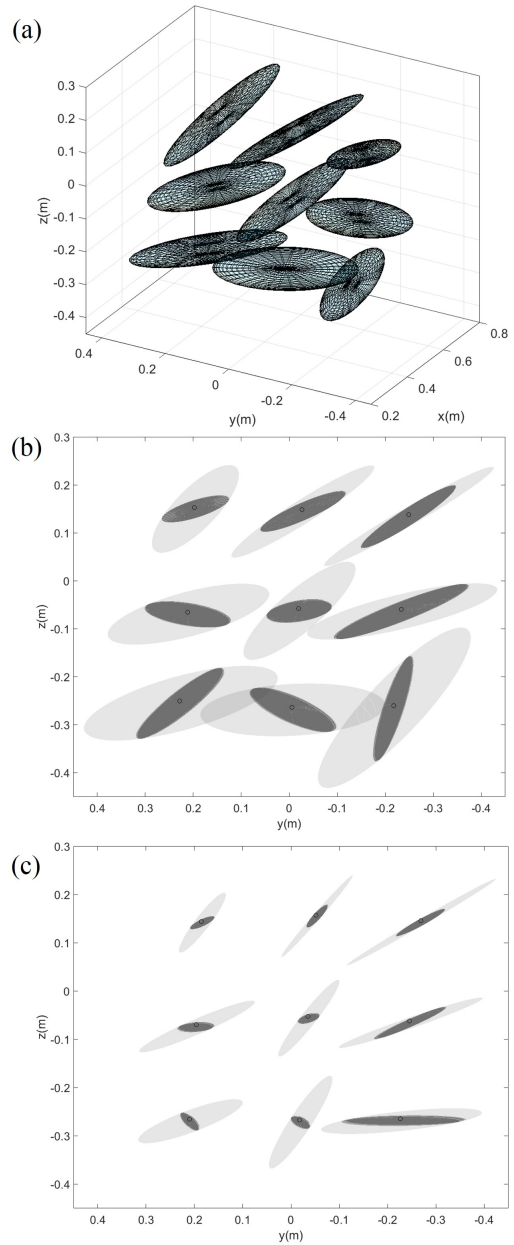

Fig. 4.   A subject's DMEs at 3×3 targets (*far* distance, $x \approx 0.5m$): (a) 0kg, 3D view; (b) 0kg, y-z view; (c) 2.72kg (6lb), y-z view. In (b) and (c), small circles show wrist positions, and DMEs' y-z projections are in light gray while DMEs' cross-sections at $x \approx 0.5m$ are in dark gray.

tablet are recorded and synchronized to a PC instantly via OneNote (Microsoft, USA). In this way, each sub-task could be studied individually even if visually overlap together. The post-processing work on the images is done using MATLAB (MathWorks, USA). All the procedures above have been conducted twice to obtain averaged results.

IV. Results & Discussion

Four aspects of upper limb movement under loading conditions are quantitatively analyzed and discussed: *manipulability*, *redundancy resolution* (i.e., swivel angles), *swivel angles vs. APSI*, and *arm's control performance*.

A. Manipulability

First, to clearly demonstrate the effects of additional loads, a subject's kinematics data at 3×3 targets, *far* distance, under two different loads of 0 and 2.72kg (= 0 and 6lb) is processed and illustrated in Fig. 4. Increasing the load shrinks ellipsoid size (manipulability measure), but also changes axes orientation and center position. The results support the intuition that an arm with additional loads would be more difficult to move, especially in some directions.

B. Swivel Angles

Effects of loading on redundancy resolution could be demonstrated by the change in swivel angles. Fig. 5 provides the swivel angle data obtained from Task I, for all ten subjects. Two 3×3 plots (a) and (b) illustrate the data at *far* and *close* distances, respectively. Each subplot (a small square) shows all ten subjects' swivel angles at that specific target, under three different loads of 0, 2.72, and 4.54kg (= 0, 6, and 10lb). Note that as shown in Fig. 3(a), the shoulder position points to the center of 3×3 targets.

A linear regression analysis is performed in Fig. 5, and it shows a consistent but counterintuitive trend at all target positions that adding loads will increase swivel angles. It means when adding loads, the elbow position will be elevated. The authors' conjecture is that as more effort is made during the shoulder flexion, a multi-joint synergy is activated.

Another observation from the data is the spatial heterogeneity of linear regression coefficients (slope and intercept) which is detailed in Fig. 6. The swivel angles at the top-right targets have the highest increasing rate (slope, deg/kg) when adding loads (*far*: 3.91, *close*: 3.80), while the lowest slope appears at the bottom-left (*far*: 0.84, *close*: 0.93). This distribution in task space may be due to obstacle (human body) collision avoidance: when wrist is at top-right target the arm has much more swivel freedom than at bottom-left.

The other coefficient, intercept is actually the swivel angle when no loading is applied. The top-left targets always have the highest intercept (deg) (*far*: 30.37, *close*: 35.45), while the lowest zero-load swivel angle for the *far* posture appears at the top-right (13.06) but shifts to the middle-right for *close* posture (13.63). This, similarly, could also be explained by obstacle collision avoidance.

C. Swivel Angles vs. APSI

As pointed out in IV. B, adding loads will increase swivel angles, but one may wonder if this change in swivel angle necessarily indicates a more instable situation. This could be explained by APSI. Fig. 7 illustrates the results from one subject to show the relationship between swivel angle and APSI. For each swivel angle measured, the corresponding APSI is calculated and plotted as a "circle" ∘ in (a) *far* or a "diamond" ◇ in (b) *close*. As mentioned above, with one's wrist and shoulder fixed, the elbow could still move along a circle by changing the swivel angle. The swivel angles in this feasible range (but not actually chosen by the subject) and the corresponding APSI values are plotted and connected as
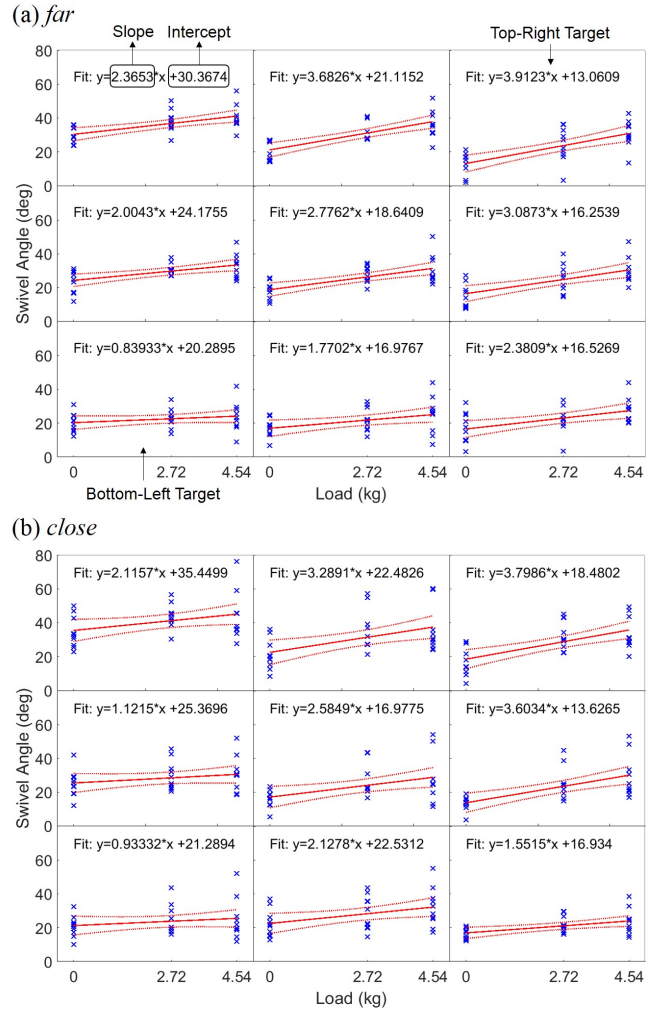

Fig. 5. Swivel angles of all ten subjects at 3×3 targets loaded with 0, 2.72 and 4.54kg: (a) *far* reach-out postures; (b) *close* reach-out postures. Cross dots with same x value represent measured data from all ten subjects under each load, and dotted lines show a 95% confidence boundary.
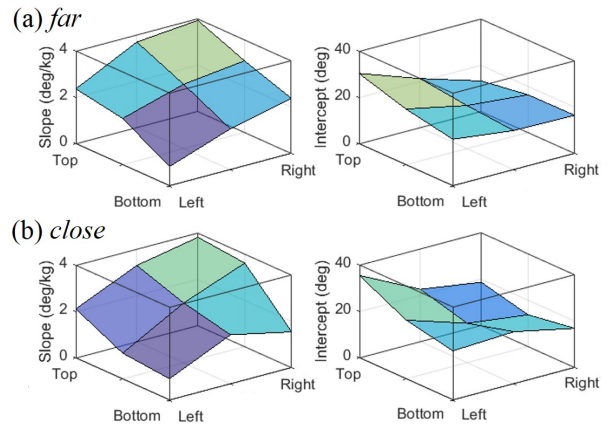

Fig. 6. Linear regression analysis from Fig. 5 shows that the swivel angle increasing rate (i.e., slope) is highest at top-right and lowest at bottom-left, for both (a) *far* and (b) *close* reach-out postures; while the swivel angle with no loading (i.e., intercept) is always at top-left.
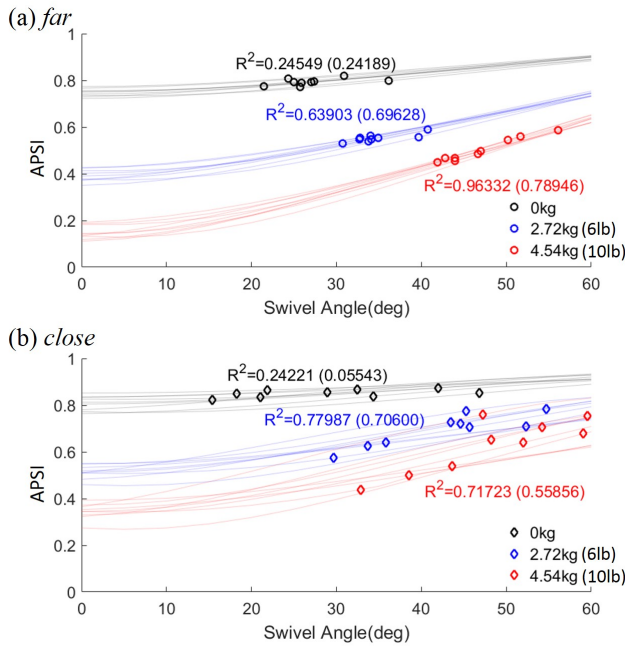
Fig. 7. Measured swivel angles at (a) *far* and (b) *close* reach-out postures and calculated APSI have a high correlation, with large loads. In other words, with large loads the swivel angle may work as a quantitative tool to differentiate spatial targets in postural stability. As the load increases, the average APSI decreases. Distribution of measured data at *far* distance is more concentrated. Circles and diamonds are experimental data, lines are computational data.
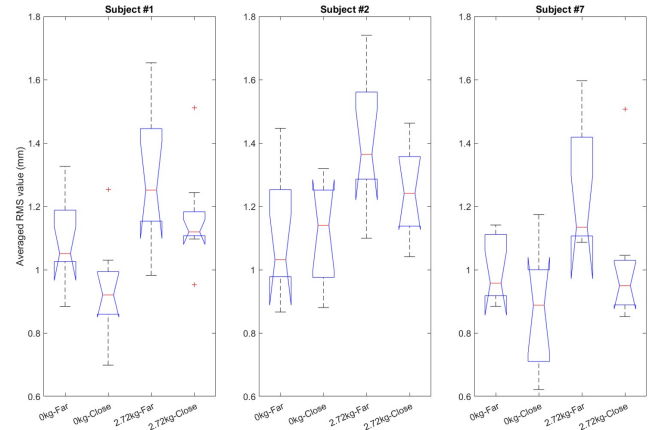

Fig. 8. Subject #1, #2 and #7: Drawing deviation (in averaged RMS value) versus loading and distance, in notched boxplots. A higher averaged RMS value indicates poorer arm's control performance.
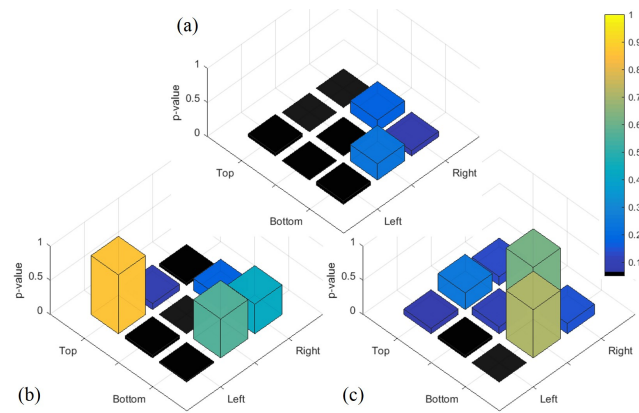

Fig. 9. P-values vary in 3×3 targets and black squares mean $p < 0.05$: (a) Load statistically influences arm control performance in most targets, concentrated at top-left; (b) Distance statistically influences arm's control performance in four out of nine targets; (c) Difference in subjects changes performance significantly in only two bottom-left targets.

individual lines via each measured data point. Under each loading condition, the R^2 value (the median of ten subjects' in brackets) from linear regression of measured swivel angle and corresponding APSI value are added to the plots.

Computationally, although both the swivel angle and its corresponding APSI are calculated very nonlinearly, there is a highly linear correlation between them, especially for *far* reach-out postures. Experimentally, higher R^2 values and a more concentrated swivel angle distribution are observed in the *far* reach-out posture than in the *close* one. Thus swivel angles under loading conditions may work as an indicator of the task difficulty.

D. Arm's Control Performance

The goal of additional Task II is to find if APSI or swivel angle could explain the arm's control performance in tasks where movement is involved.

Shown in Fig. 3(c), the root mean square (RMS) deviation of each drawing stroke from the targeted path is calculated as $d_{RMS} = \sqrt{(d_1^2 + d_2^2 + ... + d_n^2)/n}$, where d_i is the distance between a sampled point on the stylus stroke and the targeted path, n is the number of samples from target center to subtask inner circle. The RMS values for eight subtasks are averaged and its relationship with loads and distances are shown in notched boxplots in Fig. 8, which provides the data from three subjects who participated in Task II. It is found that extra loads at the *far* reach-out posture result in higher average RMS values of drawing deviation, indicating

a deterioration of arm's control performance. However, no significant correlation is observed between arm's control performance and the proposed APSI, or swivel angles.

To further understand the information embedded in the data, a three-way analysis of variance (ANOVA) is performed and p-values are illustrated in Fig. 9, where $p < 0.05$ is shown in black. Based on the three-way ANOVA, the p-value distributions in Fig. 9 show that (a) load significantly influences the performance in most targets, but (b) the distance between the subject and target plane does not, statistically, play a strong role in more than half of the targets. This might be due to the human arm's inherent tremor, when no additional load is present. No significant difference is observed among subjects, except at the bottom-left targets. The authors consider that the possible arm-body collision avoidance strategy dominates here.

E. Model Simplifications in the Study

In this study, for computational efficiency a dynamical manipulability ellipsoid (DME) model was chosen although a

force polytope (FP) model that uses a hypercube joint torque constraint may better describe the heterogeneity of arm capabilities in space [23]. Also, since joint torque capabilities change with joint angles, a $\mathbf{q}$-dependent T matrix might be more accurate [7].

V. Conclusion & Future Applications

In this paper, the human arm redundancy resolution under gravitational loading conditions is quantitatively studied. Additional loading does change the arm's movement in several aspects like manipulability and redundancy resolution strategy. A new scalar index describing the arm postural stability (APSI) is proposed and the authors conjecture that swivel angle may work as an indicator of the arm postural stability and task difficulty. The load-induced effects observed in this study may lend important referential information for designing force and position controllers of redundant robotic exoskeleton systems used for resistance rehabilitation training and assist-as-needed gravity compensation. The model and findings may also be extended to general humanoid research and applications including human-like motion controller design.

Appendix

For readers' reference, each entry of the Jacobian matrix $J_{3\times4}$ is provided below.

$$j_{11} = s1c3s4L_2 - c1s2s3s4L_2 - c1c2L_1 - c1c2c4L_2 \quad (13)$$

$$j_{12} = -s1c2s3s4L_2 + s1s2L_1 + s1s2c4L_2 \quad (14)$$

$$j_{13} = c1s3s4L_2 - s1s2c3s4L_2 \quad (15)$$

$$j_{14} = -c1c3c4L_2 - s1s2s3c4L_2 + s1c2s4L_2 \quad (16)$$

$$j_{21} = 0 \quad (17)$$

$$j_{22} = s2s3s4L_2 + c2L_1 + c2c4L_2 \quad (18)$$

$$j_{23} = -c2c3s4L_2 \quad (19)$$

$$j_{24} = -c2s3c4L_2 - s2s4L_2 \quad (20)$$

$$j_{31} = s1s2s3s4L_2 + c1c3s4L_2 + s1c2L_1 + s1c2c4L_2 \quad (21)$$

$$j_{32} = -c1c2s3s4L_2 + c1s2L_1 + c1s2c4L_2 \quad (22)$$

$$j_{33} = -c1s2c3s4L_2 - s1s3s4L_2 \quad (23)$$

$$j_{34} = -c1s2s3c4L_2 + s1c3c4L_2 + c1c2s4L_2 \quad (24)$$

Acknowledgment

References

[1] D. Mozaffarian et al., "Heart Disease and Stroke Statistics - 2016 Update: A Report From the American Heart Association," Tech. Rep., 2016.

[2] C. Patten, J. Lexell, and H. E. Brown, "Weakness and strength training in persons with poststroke hemiplegia: Rationale, method, and efficacy," *J. Rehabil. Res. Dev.*, vol. 41, no. 3A, pp. 293–312, 2004.

[3] J. H. Cauraugh, S. A. Coombes, N. Lodha, and J. J. Summers, "Upper extremity improvements in chronic stroke: Coupled bilateral load training," *Restor. Neurol. Neurosci.*, vol. 27, no. 1, pp. 17–25, 2009.

[4] T. Nef, M. Mihelj, G. Kiefer, C. Perndl, R. Müller, and R. Riener, "ARMin - Exoskeleton for arm therapy in stroke patients," in *Proc. 2007 IEEE 10th Int. Conf. Rehabil. Robot.*, 2007, pp. 68–74.

[5] N. N. Byl, G. M. Abrams, E. Pitsch, I. Fedulow, H. Kim, M. Simkins, S. Nagarajan, and J. Rosen, "Chronic stroke survivors achieve comparable outcomes following virtual task specific repetitive training guided by a wearable robotic orthosis (UL-EXO7) and actual task specific repetitive training guided by a physical therapist," *J. Hand Ther.*, vol. 26, no. 4, pp. 343–352, 2013.

[6] T. Proietti, V. Crocher, A. Roby-Brami, and N. Jarrasse, "Upper-limb robotic exoskeletons for neurorehabilitation: a review on control strategies," *IEEE Rev. Biomed. Eng.*, vol. 9, pp. 4–14, 2016.

[7] M. Sasaki, T. Iwami, K. Miyawaki, I. Sato, G. Obinata, and A. Dutta, "Higher Dimensional Spatial Expression of Upper Limb Manipulation Ability based on Human Joint Torque Characteristics," in *Robot Manip. New Achiev.*, 2010, pp. 693–719.

[8] J. Jacquier-Bret, P. Gorce, and N. Rezzoug, "The manipulability: a new index for quantifying movement capacities of upper extremity," *Ergonomics*, vol. 55, no. 1, pp. 69–77, 2012.

[9] Y. Tanaka, K. Nishikawa, N. Yamada, and T. Tsuji, "Analysis of Operational Comfort in Manual Tasks Using Human Force Manipulability Measure," *IEEE Trans. Haptics*, vol. 8, no. 1, pp. 8–19, 2015.

[10] C. J. Walsh, K. Pasch, and H. Herr, "An autonomous, underactuated exoskeleton for load-carrying augmentation," in *IEEE Int. Conf. Intell. Robot. Syst.*, 2006, pp. 1410–1415.

[11] K. E. Gordon, M. Wu, J. H. Kahn, Y. Y. Dhaher, and B. D. Schmit, "Ankle load modulates hip kinetics and EMG during human locomotion." *J. Neurophysiol.*, vol. 101, no. 4, pp. 2062–2076, 2009.

[12] Y. Yu and W. Liang, "Design optimization for lower limb assistive mechanism based on Manipulability Inclusive Principle," *Proc. 2012 IEEE Int. Conf. Robot. Biomimetics*, pp. 174–180, 2012.

[13] A. Gupta, M. K. O'Malley, V. Patoglu, and C. Burgar, "Design, Control and Performance of RiceWrist: A Force Feedback Wrist Exoskeleton for Rehabilitation and Training," *Int. J. Rob. Res.*, vol. 27, no. 2, pp. 233–251, 2008.

[14] F. J. Valero-Cuevas, "A Mathematical Approach to the Mechanical Capabilities of Limbs and Fingers," in *Prog. Mot. Control*, D. Sternad, Ed. Springer US, 2009, pp. 619–633.

[15] H. Endo, "Application of robotic manipulability indices to evaluate thumb performance during smartphone touch operations," *Ergonomics*, vol. 58, no. 5, pp. 736–747, 2015.

[16] T. Yoshikawa, "Analysis and Control of Robot Manipulators with Redundancy," in *Robot. Res. First Int. Symp.* Cambridge, MA, US: MIT Press, 1984, pp. 735–747.

[17] P. Chiacchio, S. Chiaverini, L. Sciavicco, and B. Siciliano, "Influence of Gravity on the Manipulability Ellipsoid for Robot Arms," *J. Dyn. Syst. Meas. Control*, vol. 114, no. 4, pp. 723–727, 1992.

[18] T. Yoshikawa, "Manipulability and redundancy control of robotic mechanisms," *Proceedings. 1985 IEEE Int. Conf. Robot. Autom.*, vol. 2, pp. 1004–1009, 1985.

[19] S. L. Chiu, "Task Compatibility of Manipulator Postures," *Int. J. Rob. Res.*, vol. 7, no. 5, pp. 13–21, 1988.

[20] P. Chiacchio, "A new dynamic manipulability ellipsoid for redundant manipulators," *Robotica*, vol. 18, no. 04, pp. 381–387, 2000.

[21] S. Plagenhoef, F. G. Evans, and T. Abdelnour, "Anatomical Data for Analyzing Human Motion," *Res. Q. Exerc. Sport*, vol. 54, no. 2, pp. 169–178, 1983.

[22] J. C. Perry, J. Rosen, and S. Burns, "Upper-limb powered exoskeleton design," *IEEE/ASME Trans. Mechatronics*, vol. 12, no. 4, pp. 408–417, 2007.

[23] R. Finotello, T. Grasso, G. Rossi, and A. Terribile, "Computation of kinetostatic performances of robot manipulators with polytopes," *Proc. 1998 IEEE Int. Conf. Robot. Autom.*, pp. 3241–3246, 1998.